How to cite: *Angew. Chem. Int. Ed.* **2024**, *63*, e202314238
doi.org/10.1002/anie.202314238

Theoretical Chemistry

Confined Lewis Pairs: Investigation of the $X^- \rightarrow Si_{20}$ Interaction in Halogen-Encapsulating Silafulleranes

Thomas Gasevic[+], *Marcel Bamberg*[+], *Julius Wicke, Michael Bolte, Alexander Virovets, Hans-Wolfram Lerner, Stefan Grimme, Andreas Hansen,* Matthias Wagner,* and Markus Bursch**

Abstract: A joint theoretical and experimental study on 32 endohedral silafullerane derivatives $[X@Si_{20}Y_{20}]^-$ (X = F-I; Y = F-I, H, Me, Et) and T_h-$[Cl@Si_{20}H_{12}Y_8]^-$ (Y = F-I) is presented. First, we evaluated the structure-determining template effect of Cl^- in a systematic series of concave silapolyquinane model systems. Second, we investigated the $X^- \rightarrow Si_{20}$ interaction energy (E_{int}) as a function of X^- and Y and found the largest E_{int} values for electron-withdrawing exohedral substituents Y. Given that X^- ions can be considered as Lewis bases and empty $Si_{20}Y_{20}$ clusters as Lewis acids, we classify our inseparable host–guest complexes $[X@Si_{20}Y_{20}]^-$ as "confined Lewis pairs". Third, ^{35}Cl NMR spectroscopy proved to be highly diagnostic for an experimental assessment of the $Cl^- \rightarrow Si_{20}$ interaction as the paramagnetic shielding and, in turn, $\delta(^{35}Cl)$ of the endohedral Cl^- ion correlate inversely with E_{int}. Finally, we disclose the synthesis of $[PPN][Cl@Si_{20}Y_{20}]$ (Y = Me, Et, Br) and provide a thorough characterization of these new silafulleranes.

Introduction

Mapping the similarities and differences between carbon and its heavier homolog silicon is a central theme in main group chemistry.[1] Therefore, mimicking structural motifs with silicon that are known from carbon-containing molecules has become a fundamental motivation for the synthesis of new silicon compounds.[2–4] Shortly after their discovery, fullerenes (C_{20}-C_{70}; Kroto, Smalley, Krätschmer, Prinzbach *et al.*, 1985)[5–9] and dodecahedrane ($C_{20}H_{20}$; Paquette *et al.*, 1982)[10] were considered milestones in the field of nanoscience and sparked a growing interest also in spherical molecules made of silicon atoms. However, this compound class remained synthetically inaccessible for a long time. A special interest arose for the smallest possible silafullerene I_h-Si_{20} after Prinzbach *et al.* were able to generate the carbonaceous congener C_{20} in the gas phase.[8] Since calculations suggested that the dodecahedral Si_{20} cage is not stable but should collapse into more compact structures,[11–16] the following strategies for its stabilization were postulated by theory: (i) encapsulation of formally neutral or charged guests $X^{n+/n-}$ to obtain endohedral complexes $[X@Si_{20}]^{n+/n-}$ (e.g., $X^{n+/n-} = Ba^0$, Zr^0, U^{6-}),[17–22] (ii) exohedral saturation by switching from the silafullerene Si_{20} to a silafullerane $Si_{20}Y_{20}$ (e.g., Y = H),[23–36] or (iii) the combination of both approaches leading to endohedral silafulleranes $[X@Si_{20}Y_{20}]^{n+/n-}$ (e.g., $X^{n+/n-} = Li^+$, Cl^-, O^{2-}; Y = H, F).[37–42]

In 2015, the Wagner group finally discovered a one-step protocol for the synthesis of the [20]silafullerane T_h-$[Cl@Si_{20}(SiCl_3)_{12}Cl_8]^-$, which was isolated as the tetraalkylammonium salt $[R_4N][\mathbf{A}]$ (R = Et, *n*Bu; Figure 1).

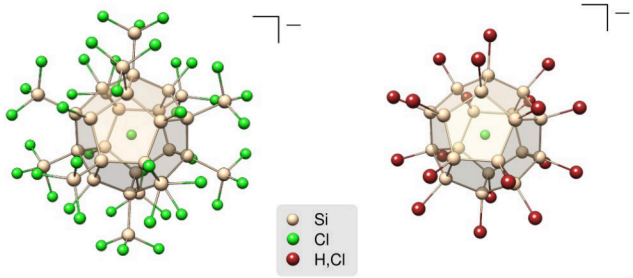

$[Cl@Si_{20}(SiCl_3)_{12}Cl_8]^-$ ($[\mathbf{A}]^-$) $[Cl@Si_{20}Y_{20}]^-$ ($[\mathbf{B}]^-$)

Figure 1. Molecular structures of the [20]silafulleranes $[\mathbf{A}]^-$ and $[\mathbf{B}]^-$.

[*] T. Gasevic,[+] Prof. Dr. S. Grimme, Dr. A. Hansen
Mulliken Center for Theoretical Chemistry,
University of Bonn
Beringstraße 4, 53115 Bonn (Germany)
E-mail: hansen@thch.uni-bonn.de

Dr. M. Bamberg,[+] J. Wicke, Dr. M. Bolte, Dr. A. Virovets,
Dr. H.-W. Lerner, Prof. Dr. M. Wagner
Institut für Anorganische und Analytische Chemie,
Goethe-Universität Frankfurt am Main
Max-von-Laue-Straße 7, 60438 Frankfurt am Main (Germany)
E-mail: matthias.wagner@chemie.uni-frankfurt.de

Dr. M. Bursch
Max-Planck-Institut für Kohlenforschung
Kaiser-Wilhelm-Platz 1, 45470 Mülheim an der Ruhr (Germany)
E-mail: bursch@kofo.mpg.de

[+] These authors contributed equally.

$[\mathbf{A}]^-$ contains a dodecahedral Si_{20} core with endohedral Cl^- guest and is exohedrally saturated by 12 $SiCl_3$ and 8 Cl substituents, hence following design principle (iii).[43] Recently, $[\mathbf{A}]^-$ was converted into the T_h-symmetric, mixed-substituted $[Cl@Si_{20}H_{12}Cl_8]^-$ and into a variety of $[Cl@Si_{20}Y_{20}]^-$ derivatives ($[n\mathrm{Bu_4N}][\mathbf{B}]$; Y = H, Cl; Figure 1).[44] These experimental results proved that $Si_{20}Y_{20}$ cages, which according to calculations of Goedecker *et al.* (Y = H) should be hardly accessible,[45] can be made accessible by Cl^- encapsulation. This result immediately raises the question of whether the Si_{20} dodecahedron is assembled around the Cl^- ion and to what extent this endohedral guest exerts a structure-determining template effect. In this context, the nature and the degree of the $Cl^- \rightarrow Si_n$ interaction are of prime importance. Theoretical investigations by Holthausen *et al.* revealed that the formation of $[\mathbf{A}]^-$ by formal incorporation of Cl^- into the hypothetical empty cluster is exergonic by $> 100\ \mathrm{kcal\,mol^{-1}}$.[43] Ponce-Vargas and Muñoz-Castro contributed an energy decomposition analysis (EDA) of the $Cl^- \rightarrow Si_{20}$ interaction in $[\mathbf{A}]^-$ that revealed a mainly electrostatic character, which we also observed in our previous publication.[44,46]

Herein, we present a combined theoretical and experimental investigation of the cooperative effects between the endohedral ion and the exohedral decoration in [20]silafulleranes $[X@Si_{20}Y_{20}]^-$ (Figure 2). To ensure reliable results from our quantum mechanical calculations,[47–52] we assessed various density functional approximations on high-level reference data beforehand. From a theoretical perspective, we evaluate the central interaction between the endohedral ion X^- and the empty host $Si_{20}Y_{20}$. This is done for (i) small cluster fragments composed of annulated five-membered rings ("silapolyquinanes") and (ii) for $[X@Si_{20}Y_{20}]^-$ clusters with different endohedral ions (X^-) and exohedral substituents (Y). These calculations not only shed light on the role of the Cl^- ion as a structure-determining template during cluster buildup but also provide a first insight into the thermodynamics of cluster degradation.

Further, we present a thorough NMR study based on theoretical predictions of ^{35}Cl chemical shifts. We investigate parallels to the well-known Gutmann–Beckett method,

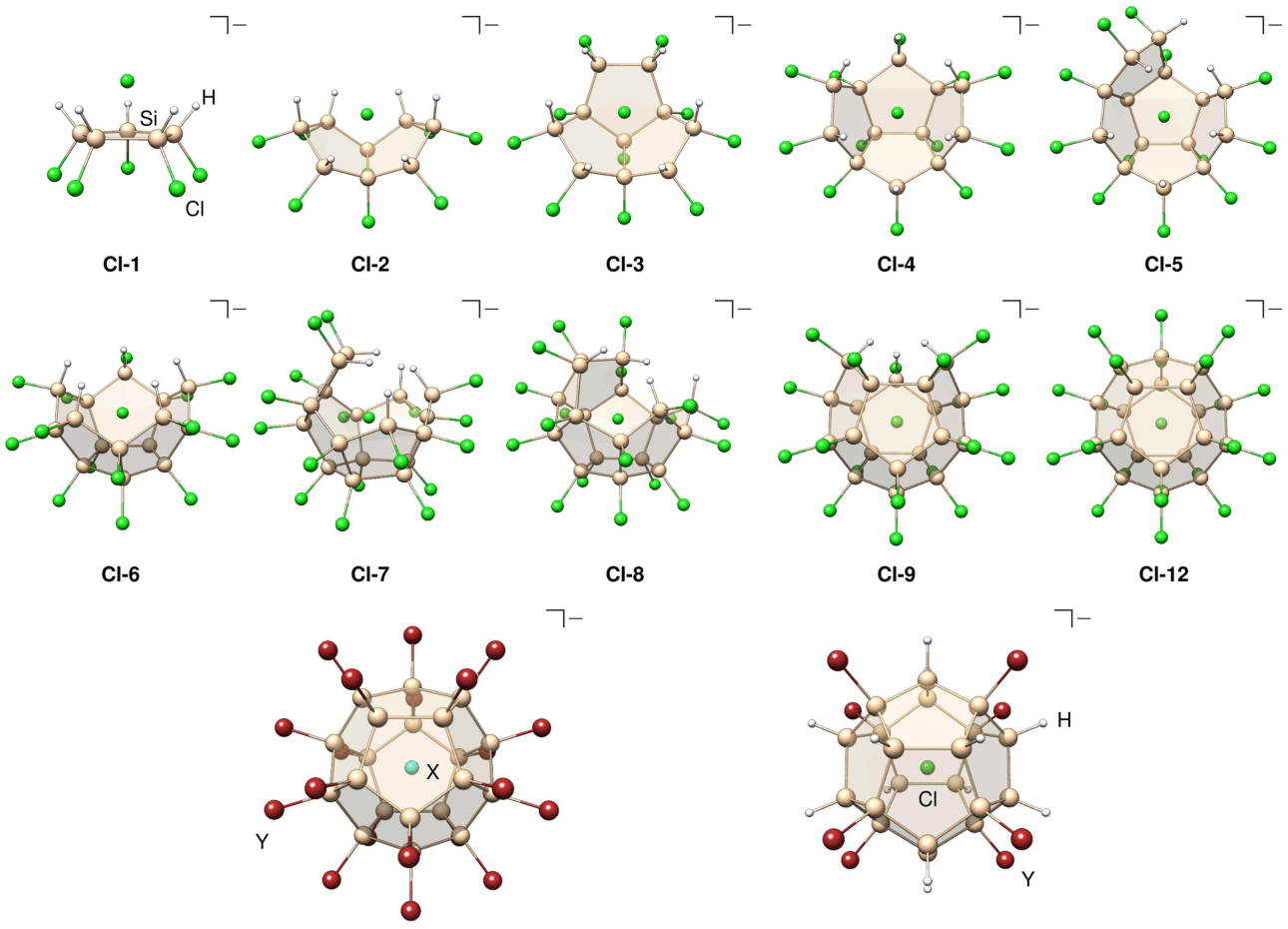

Figure 2. Computationally optimized structures (PBEh-3c(SMD(CH_2Cl_2))) of the systems relevant for the discussion.

which is used to evaluate the effective Lewis acidity of compounds by the ^{31}P NMR chemical shift of a coordinated Et_3PO sensor ligand.[53,54] For this, we compare different properties, such as the interaction energy or the donor-acceptor gap, with the respective ^{35}Cl NMR chemical shift of the silafullerane-encapsulated Cl^- ion. On the experimental side, we expand the range of synthetically available derivatives by providing the syntheses of $[Cl@Si_{20}Y_{20}]^-$ (Y = Me, Et, Br) to ultimately include systems that distribute the negative charge over an even larger volume than $[Cl@Si_{20}Cl_{20}]^-$ and those that have a lipophilic shell.

Results and Discussion

Template Effect in the Cluster Assembly

Perhalogenated cyclopentasilanes Si_5X_{10} and cyclohexasilanes Si_6X_{12} are known to be ditopic Lewis acids (LA) that coordinate Lewis bases (LB) such as nitriles (RCN) or halide ions in a μ_5 ($Si_5X_{10}\cdot 2LB$) or μ_6 ($Si_6X_{12}\cdot 2LB$) mode on both sides of the respective ring to form inverse sandwich complexes.[55–64] A similar interaction is found for the halide encapsulating $[X@Si_{20}Y_{20}]^-$ clusters, where the dissociation of the encapsulated ion is inhibited by the surrounding Si_{20} cage. Accordingly, we classify our silafulleranes as "confined Lewis pairs" with the Si_{20} cage being the Lewis acid and the endohedral ion (X^-) the Lewis base. The confinement of a Lewis base inside a molecular cage has been applied in frustrated Lewis pair (FLP) chemistry, but in those cases, the cage itself did not act as a Lewis acid.[65,66] The classification as "confined Lewis pair" is helpful to distinguish our endohedral silafulleranes from non-confined Lewis pairs such as cyclosilane-base adducts. In the following, we will investigate the intrinsic interactions and NMR properties of this newly introduced compound class of confined Lewis pairs.

The mechanism underlying the one-step synthesis of $[Cl@Si_{20}(SiCl_3)_{12}Cl_8]^-$ from Si_2Cl_6 poses a fundamentally interesting but so far unsolved problem. Since, to our best knowledge, no intermediates of the cluster assembly are known, we apply QM computations to gain some insights into the process of cluster assembly. Our central working hypothesis assigns a structure-directing template effect to the Cl^- ion that is ultimately trapped inside the cluster[43] (cf. Goedecker's conclusion that an empty $Si_{20}H_{20}$ siladodecahedrane will not form spontaneously – despite its predicted thermodynamic stability – due to Levinthal's paradox).[45] The siladodecahedrane consists exclusively of five-membered rings, and it has already been theoretically established that cyclopentasilanes are early intermediates of oligosilane "Aufbau" reactions occurring in Si_2Cl_6/Cl^- mixtures.[55] Thus, we first investigated the energetic landscape of adducts between one Cl^- ion and a successively growing concave framework of *m* mutually annulated cyclopentasilane rings. For these adducts, we will use the nomenclature "**Cl-*m***" (Figure 2; *m* = 1–12 Si_5 rings; note that **Cl-10** and **Cl-11** do not exist due to the simultaneous formation of three five-membered rings in the final step leading from **Cl-9** directly to **Cl-12**). Geometries of each adduct have been fully optimized. Generally, we used the PBEh-3c[67]-(SMD(CH_2Cl_2))[68] level of theory for the optimization of all geometries in this work. At each stage, the emerging silapolyquinane[69] scaffolds represent growing fragments of the $Si_{20}Y_{20}$ cluster (Kyushin's permethylated decasilahexahydrotriquinacene[70] is the only experimentally accessible bowl-shaped oligosilane yet known). Specifically, we began with the $[Si_5H_5Cl_5\cdot Cl]^-$ adduct **Cl-1**, in which the Cl^- anion is placed above the perhydrogenated face of the ring. For two reasons, the positions serving as anchor points for the subsequent annulation steps were saturated by H atoms: (i) H substituents have the smallest possible steric demand and (ii) the difference in electronegativity is smaller between H and Si than between Cl and Si. Although different reaction mechanisms could be possible, we focus on one of the structurally most related mechanisms. Nevertheless, it should not be taken as a proposed reaction mechanism.

For each silapolyquinane (**Cl-*m***) we modeled for the cluster assembly series, we performed a local energy decomposition (LED)[71–73] analysis at the DLPNO-CCSD(T)[74–78]/*TightPNO*/def2-TZVPP level of theory to understand the changes in the interaction energy composition upon subsequent annulation (cf. Figure 3). The LED gives rise to different contributions of the total $Cl^-\rightarrow Si_n$ interaction energy (E_{int}) and contains, e.g., the electronic preparation energy at the Hartree–Fock (HF) level ($E_{HF-elprep}$) that describes the repulsive part of the exchange interaction and can therefore be identified as "Pauli repulsion". Further components describe the electrostatic interaction (E_{elstat}), attractive exchange energy (E_{exch}), orbital-relaxation ($E_{orb-relax}$), London dispersion (E_{disp}) and non-dispersion ($E_{non-disp}$) effects. The $E_{non-disp}$ term is added as a correction to errors in the permanent electrostatic interactions inherent to the HF method. The total interaction energy is decomposed according to Eq. (1). Each contribution is computed as the difference (Δ) between the relaxed complex and the sum of the unrelaxed Si_n fragment and the endohedral ion X^-.

$$E_{int} = \Delta E_{HF-elprep} + \Delta E_{elstat} + \Delta E_{exch} + \Delta E_{orb-relax} + \Delta E_{disp} + \Delta E_{non-disp} \quad (1)$$

Overall, the total $Cl^-\rightarrow Si_n$ interaction steadily becomes stronger as the silapolyquinanes grow in size, which underlines the postulated template effect of the Cl^- ion (cf. Figure 3a). The respective interaction energies range from −78.3 (**Cl-1**) to −146.6 kcal mol^{-1} (**Cl-12**). Electron correlation contributes significantly to the interaction energy and is therefore indispensable for reliable results (see the difference between DLPNO-CCSD(T) and HF in Figure 3a). The electron correlation describes the sum of the non-dispersion and London dispersion terms found in the LED. As the London dispersion term is larger, it has a bigger influence on the overall interaction (see Supporting Information, Figure S1). The average distance between the endohedral

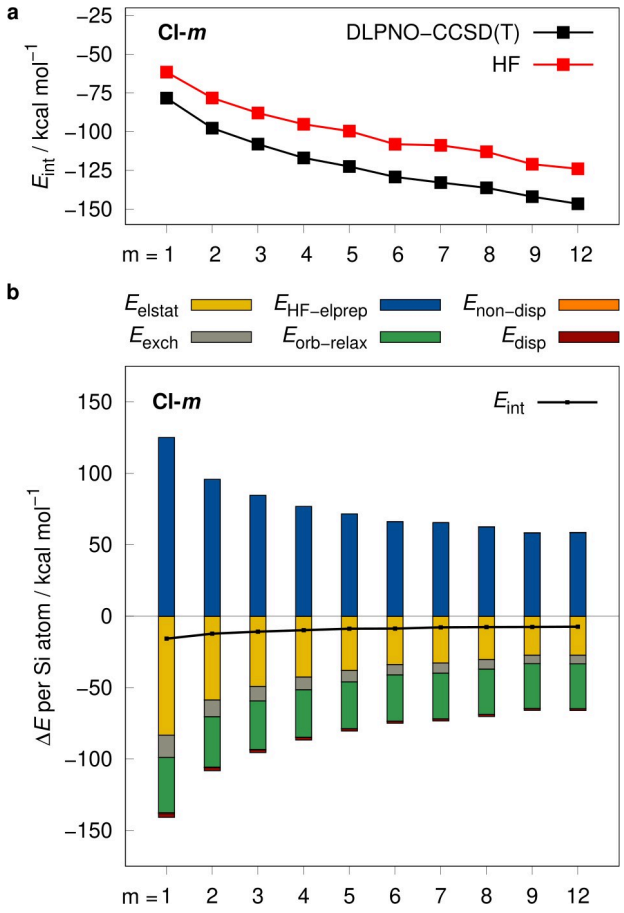

Figure 3. (a) Computed Cl→Si$_n$ interaction energy applying DLPNO-CCSD(T)/*TightPNO*/def2-TZVPP and HF/def2-TZVPP. (b) LED per Si atom for the cluster assembly series of $[Cl@Si_{20}Cl_{20}]^-$ (**Cl-*m***) computed with DLPNO-CCSD(T)/*TightPNO*/def2-TZVPP. Contributions of $E_{non-disp}$ are in a range between −0.83 and 0.16 kcal mol^{-1} and therefore not visible.

Cl^- ion and the centers of the five-membered Si rings increases with the size of the silapolyquinanes and it therefore correlates with the interaction strength (Table 1). In the same series, the bond lengths between the Si atoms and the exohedral Cl substituents become subsequently smaller, and the positive partial charge of the Si atoms is reduced. As the silapolyquinanes grow in size, there are more available interaction sites, which leads to an increased interaction strength. A more detailed overview of the interaction can be obtained by analyzing each contribution with respect to the number of Si atoms n in the molecule (cf. Figure 3b). With increasing cluster size, each contribution to E_{int} per Si atom is decreasing as the Cl^-→Si$_n$ interaction is distributed among more atom pairs. This indicates the importance of many-body effects for the overall interaction. London dispersion and non-dispersion effects are very small compared to the remaining contributions and are almost negligible. Contributions from the attractive exchange interaction are slightly larger but still small compared to the remaining contributions. During the cluster assembly, the orbital-relaxation per Si atom is the only contribution that is almost constant as each silapolyquinane has a similar orbital overlap between the endohedral Lewis base and the Si center due to high symmetry. The main repulsive interaction is the Pauli repulsion, while the main attractive interactions are orbital-relaxation effects and electrostatics. This is in line with the previous theoretical study on $[X@Si_{32}Cl_{44}]^-$ by Muñoz-Castro *et al.*, which points out the dominant electrostatic character of the Cl^-→Si_{20} interaction.[46]

Interplay of Endohedral Ion and Exohedral Substitution

In the next sections, we will discuss the influence of different endohedral ions and exohedral substituents on the electronic X^-→Si_{20} interaction. For this, we modeled $[X@Si_{20}Y_{20}]^-$ clusters with the endohedral ions X = F, Cl, Br, I and the exohedral substituents Y = F, Cl, Br, I, H, Me, Et (Figure 2). Additionally, we included the partially substituted $[Cl@Si_{20}H_{12}Y_8]^-$, Y = F, Cl, Br, I clusters.

The X^-→Si_{20} interaction is the most important one in our tested systems. It is given as the electronic energy difference between the $[X@Si_{20}Y_{20}]^-$ cluster and the sum of the unrelaxed fragments X^- and $Si_{20}Y_{20}$. We computed the corresponding interaction energies at the most accurate level of theory, which was still affordable given the complexity

Table 1: Average distances between the endohedral Cl^- ion and the centers of the five-membered Si rings (c(Si_5)) as well as the average distances between the Si atoms and the exohedral Cl substituents, and the average of natural charges in the molecules **Cl-*m***.

	av. distances/Å		av. natural charges/e$^-$		
	$d(Cl^-\cdots c(Si_5))$	d(Si–Cl)	Cl^-	Si	Cl
Cl-1	2.1473	2.1097	−0.531	0.467	−0.416
Cl-2	2.2740	2.0955	−0.497	0.432	−0.387
Cl-3	2.3383	2.0895	−0.486	0.409	−0.373
Cl-4	2.3914	2.0859	−0.479	0.392	−0.364
Cl-5	2.4532	2.0360	−0.472	0.381	−0.357
Cl-6	2.5090	2.0808	−0.484	0.365	−0.351
Cl-7	2.5111	2.0800	−0.461	0.358	−0.347
Cl-8	2.5641	2.0784	−0.468	0.346	−0.343
Cl-9	2.6269	2.0764	−0.486	0.335	−0.339
Cl-12	2.6206	2.0742	−0.468	0.307	−0.333

and size of the systems (PNO-LCCSD(T)-F12b[79–81]/AVTZ'/default including scaled triples contributions to approximate PNO-LCCSD(T)-F12b/AVQZ'/tight results).[82–86] More details can be found in section 1.2 of the Supporting Information. Although estimated results with centered, endohedral F^- ions are presented, it is worth mentioning that these compounds have imaginary modes up to 100 cm^{-1} for the endohedral ion movement indicating unstable structures that cannot be isolated experimentally. Since we investigate the interaction between centered endohedral ions and the Si moieties, these structures still yield valuable information for the evaluation of [20]silafulleranes. We included them in our studies, but we will not focus on these compounds in the following.

For the mixed-substituted $[Cl@Si_{20}H_{12}Y_8]^-$ clusters, we observe no significant change in E_{int} with different exohedral halogen substituents Y and will therefore omit them in the following energy discussion (cf. Supporting Information, Figure S2). In the fully substituted derivatives $[X@Si_{20}Y_{20}]^-$, small E_{int} were computed for systems with Y = H, Me, Et, while large E_{int} were computed for Y = Halogen (cf. Figure 4). As described in the previous section, the main attractive contribution to the $X^- \rightarrow Si_{20}$ interaction is of electrostatic origin. Therefore, the largest E_{int} is expected for a system with a hard Lewis base in the endohedral position and an electron-poor Si_{20} cage, which can be achieved, e.g., with inductively electron-withdrawing halogen substituents. Based on our calculations we predict the weakest E_{int} for $[I@Si_{20}Et_{20}]^-$ and the strongest E_{int} for $[F@Si_{20}F_{20}]^-$ within our test set. Since $[F@Si_{20}F_{20}]^-$ is no minimum structure, $[Cl@Si_{20}F_{20}]^-$ can be regarded as having the strongest interaction energy in our test set.

The interaction energy (E_{int}) only consists of the electronic energy (E_{el}), but experimentally measured properties also include solvation (δG_{solv}) and thermostatistical contributions (G_{RRHO}) which we computed with COSMO-RS[87–90] and the thermo submodule of XTB,[91] respectively. These corrections can be directly added to the electronic energy which leads to the total Gibbs free energy (G) according to Eq. (2). Each contribution is calculated as the difference (Δ) between the complex, the Si_{20} fragment, and the endohedral ion. In contrast to the interaction energy, each contribution is computed for fully optimized geometries and therefore it also includes geometrical relaxation effects.

$$\Delta G = \Delta E_{el} + \Delta G_{RRHO} + \Delta \delta G_{solv} \quad (2)$$

As different QM methods with varying accuracy can be applied for E_{el}, it is important to validate them beforehand. Based on our previously discussed reference values, we assessed different density functional approximations[92–110] and we selected the hybrid density functional r^2SCAN0-D4[94,95,102] in combination with the def2-QZVPPD[111] (on X^-), def2-TZVPPD (on Si), and def2-QZVPP[112] (on Y) basis sets for all further discussed results. More details can be found in the Computational Details section of the Supporting Information.

Due to the strong Si–Si cage bonds, it is practically impossible to chemically extract the endohedral ions from the Si_{20} cages, i.e., to separate the confined Lewis pair. Nevertheless, we can theoretically predict association free energies (ΔG) for this process (cf. Figure 5). Since the main difference between ΔG and E_{int} is just the solvation and thermostatistical contributions, the main trends for both are similar: systems with a hard Lewis base as endohedral ion and electron-withdrawing substituents are generally more stable and systems with positive inductive substituents are less stable. Solvation and thermostatistical contributions counteract the attractive electronic interaction and thus can also cause thermodynamically unstable structures. The most stable structures investigated are $[Br@Si_{20}F_{20}]^-$ ($\Delta G = -91.4$ kcal mol^{-1}) and $[Cl@Si_{20}F_{20}]^-$ ($\Delta G = -89.6$ kcal mol^{-1}), while the most unstable structure is $[I@Si_{20}Et_{20}]^-$ ($\Delta G = 13.2$ kcal mol^{-1}) among the investigated systems. Overall, solvation and thermostatistics have a large impact on the free energy of association in [20]silafulleranes with endohedral ions.

By encapsulation of an endohedral ion, the $Si_{20}Y_{20}$ fragment of the adduct will be distorted compared to an empty $Si_{20}Y_{20}$ cage; we term the corresponding energies $E_{cage,adduct}$ and $E_{cage,relaxed}$, respectively. We computed the geometric change in cluster width as well as cage strain (E_{strain}) in each investigated complex (cf. Figure 6) according to Eq. (3).

$$E_{strain} = E_{cage,adduct} - E_{cage,relaxed} \quad (3)$$

In most systems, the Si_{20} cage is contracted upon encapsulation of an endohedral ion due to the attractive $X^- \rightarrow Si_{20}$ interaction.

Only for some combinations of the larger endohedral ions Br^- and I^- with less electron-withdrawing cluster

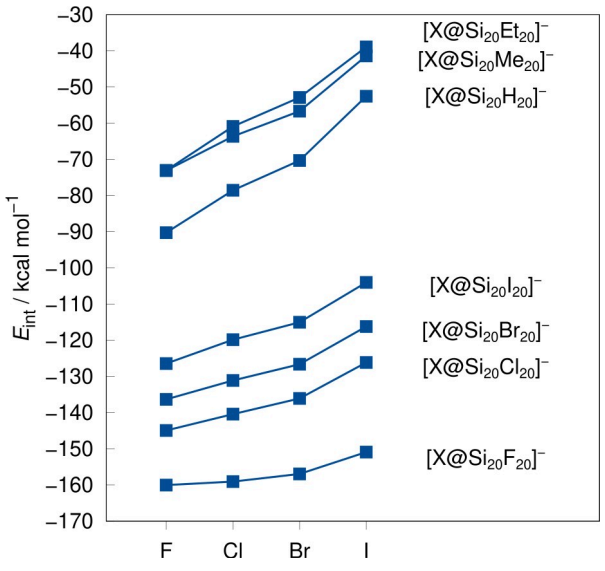

Figure 4. Computed interaction energies (E_{int}) for the $X^- \rightarrow Si_{20}$ bonds at PNO-LCCSD(T)-F12b/AVTZ'/default level including scaled triples contributions. $[X@Si_{20}Et_{20}]^-$ was computed with our best-performing density functional approximation (cf. Supporting Information).

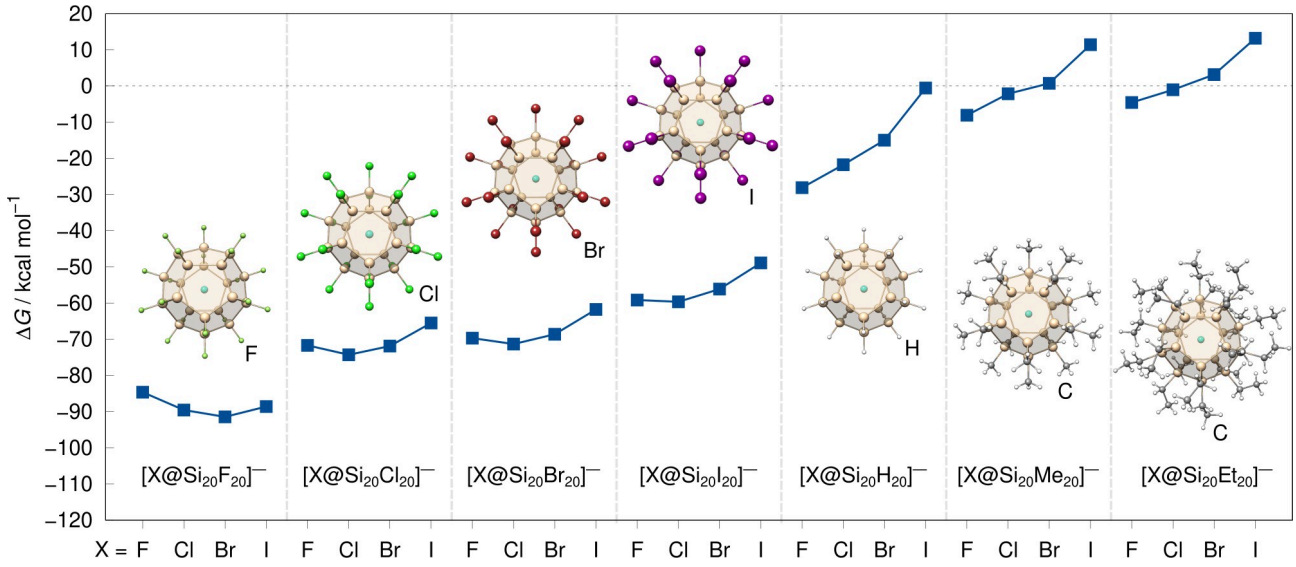

Figure 5. Gibbs free energies (ΔG) for the encapsulation of the respective endohedral ion in Si_{20} cages with different substituents computed with our best-performing DFT method (see Supporting Information).

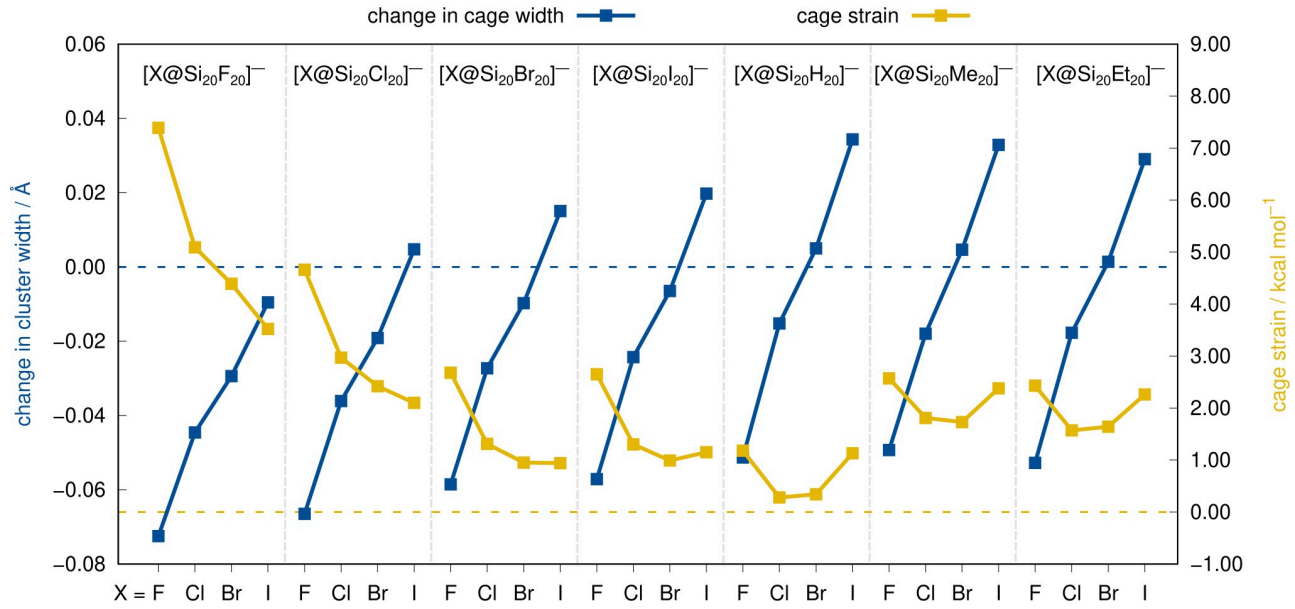

Figure 6. Change in cage width between the Si_{20} cluster fragment in $[X@Si_{20}Y_{20}]^-$ and the empty cage $Si_{20}Y_{20}$ (blue) and the corresponding cage strain (yellow) computed with our best-performing DFT method (see Supporting Information).

substituents, we observe an expansion of the cage (cf. $[I@Si_{20}Me_{20}]^-$). Generally, the cage strain correlates inversely with cage contractions and directly with cage expansions. The most contracted system is $[Cl@Si_{20}F_{20}]^-$ with a cage strain of 5.1 kcal mol^{-1} and the most expanded system is $[I@Si_{20}H_{20}]^-$ with a cage strain of only 1.1 kcal mol^{-1}.

To further investigate the effect of steric bulk on the $X^- \rightarrow Si_{20}$ interaction in $[X@Si_{20}Y_{20}]^-$, we conducted an energy decomposition analysis (EDA) at the B3LYP–D4/def2-QZVPPD level of theory for selected clusters (cf. Figure 7).[113] The EDA is similar to the previously discussed LED analysis but is computationally less demanding and can therefore also be applied to larger structures. The EDA is based on density functional theory instead of wavefunction theory, which is used in the LED. This results in slightly different contributions to the total interaction energy. The EDA includes a repulsion (E_{rep}), electrostatic (E_{elstat}), exchange (E_{exch}), orbital-relaxation ($E_{orb-relax}$), electron correlation (E_{correl}), and dispersion (E_{disp}) contributions to the total energy.

The influence of the exohedral substituent on the $Cl^- \rightarrow Si_{20}$ interaction is significantly smaller than that of the endohedral ion. The less electron-withdrawing exohedral substituents (Y = H, Me, Et) cause a stronger repulsion and

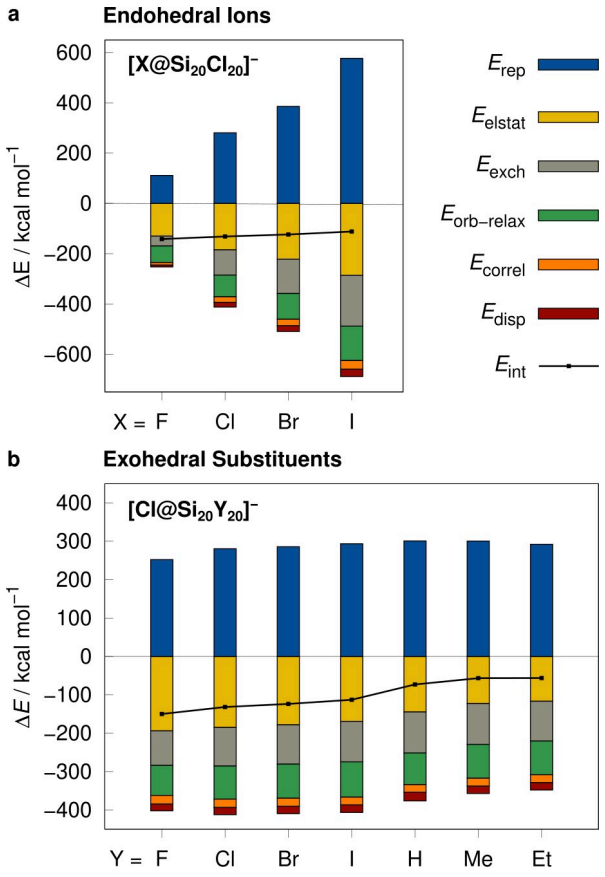

Figure 7. EDA for complexes with (a) different endohedral ions $[X@Si_{20}Cl_{20}]^-$ and (b) exohedral substituents $[Cl@Si_{20}Y_{20}]^-$.

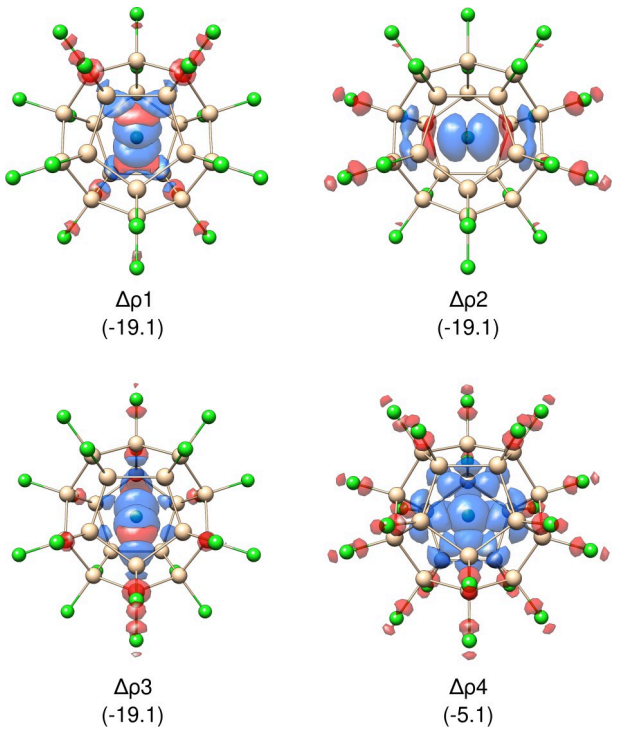

Figure 8. Deformation density difference ($\Delta\rho$) of the main contributions to the charge transfer found in $[Cl@Si_{20}Cl_{20}]^-$ and the respective energy contributions (ΔE_k) in parenthesis [kcal mol^{-1}]. Blue represents depletion and red represents expansion of density. An isosurface value of 0.0015 a.u. was applied.

a less attractive electrostatic interaction leading to an overall lower total interaction energy. The repulsion is slightly lower for the electron-withdrawing substituents (Y = F, Cl, Br, I) leading to an overall more attractive interaction.

As the endohedral ion is directly involved in the investigated interaction, the influence of the nature of X^- on the individual contributions to E_{int} is much larger than that of Y. For example, going from F^- (E_{rep} = 111.0 kcal mol^{-1}) to Cl^- (E_{rep} = 280.6 kcal mol^{-1}), the repulsion energy is more than twice as large. All EDA contributions are increasing as the endohedral ion becomes larger, whereas the total interaction energy decreases. Since the increase in repulsion is larger than the gain in attractive contributions, there is a net unfavorable effect of larger endohedral ions on E_{int}.

In order to analyze the effect of charge transfer in our tested systems, we computed deformation density differences from Natural Orbitals for Chemical Valence (NOCV)[114,115] and applied the Extended Transition State (ETS)[116] method at the same level of theory as applied in our electronic energy calculations to obtain corresponding energy contributions (ΔE_k, cf. Figure 8).[117] Since the nature of the donor and acceptor orbitals is similar for all systems investigated, we only discuss the results for the $[Cl@Si_{20}Cl_{20}]^-$ cluster exemplarily. Charge transfer mainly takes place by electron-density donation from the p_x, p_y, and p_z orbitals of the endohedral Cl^- to the σ^*(Si–Cl) orbitals of the exohedral Cl substituents which are located in the same axis. The charge transfer contribution of each p orbital is −19.1 kcal mol^{-1} ($\Delta\rho1$, $\Delta\rho2$, $\Delta\rho3$). We also observe a fourth contribution coming from the s orbital of the endohedral Cl^-, which donates electron density to the σ^* orbitals of the exohedrally located chlorine atoms, but this contribution is significantly smaller ($\Delta\rho4$, ΔE_k = −5.1 kcal mol^{-1}). These findings are in line with prior studies on [20]silafulleranes.[118]

NMR Chemical Shifts

In our previous publication on silafulleranes $[Cl@Si_{20}Y_{20}]^-$,[44] we have already found some evidence that experimentally determined ^{35}Cl NMR chemical shift values are diagnostic for a number of important properties, such as the $Cl^- \rightarrow Si_{20}$ interaction energies or the main donor-acceptor orbital gaps. Back then, however, these studies had to be limited to the three derivatives that were synthetically accessible at the time. Since a much wider palette of silafulleranes is now available, we revisit the topic in the following and confirm the correlations between $\delta(^{35}Cl)$ and key silafullerane features on a broader basis. A new aspect arises from our classification of endohedral silafulleranes $[Cl@Si_{20}Y_{20}]^-$ as confined Lewis pairs: if we take the $Cl^- \rightarrow Si_{20}$ interactions as a measure of the Lewis acidities of different empty siladodecahedranes $Si_{20}Y_{20}$, their

quantification by ^{35}Cl NMR spectroscopy is reminiscent of the well-established method of Gutmann and Beckett.[53,54] They used the difference $\Delta\delta(^{31}P)$ between $\delta(^{31}P)$ of the free sensor Lewis base Et_3PO and $\delta(^{31}P)$ of the adduct $Et_3PO{\rightarrow}$LA to assess the acidity of a given Lewis acid LA. Generally speaking, the computed chemical shift δ of a given nucleus (here: ^{35}Cl) is the difference between the total isotropic shielding of this nucleus in a reference compound (here: CH_2Cl_2; $\sigma_{tot,ref}$) and in the compound under study ($\sigma_{tot,comp}$; Eq. (4)). Each total shielding (σ_{tot}) is the sum of diamagnetic (σ_{dia}), paramagnetic (σ_{para}), and spin-orbit contributions (σ_{so}) (Eq. (5)).[119,120]

$$\delta = \sigma_{tot,ref} - \sigma_{tot,comp} \quad (4)$$

$$\sigma_{tot} = \sigma_{dia} + \sigma_{para} + \sigma_{so} \quad (5)$$

The diamagnetic contributions are derived from the unperturbed electron density and thus mainly depend on the ground state density. The paramagnetic shielding constant is related to frontier orbital transitions which renders it highly responsive to the chemical environment, including bonding and other interactions.[121] For the computation of the ^{35}Cl NMR chemical shieldings we applied the SO-ZORA[122–124] -PBE0/TZP[125] level of theory and applied the COSMO solvation model for CH_2Cl_2.[126] First, we emphasize that the theoretically and experimentally obtained $\delta(^{35}Cl)$ values of all our silafulleranes $[Cl@Si_{20}Y_{20}]^-$ are in agreement with each other; the subsequent discussion refers exclusively to calculated chemical shift data. As shown in Figure 9, the σ_{tot} values (and hence $\delta(^{35}Cl)$) of $[Cl@Si_{20}Y_{20}]^-$ are mainly determined by σ_{para}, which is much more influenced by the nature of Y than σ_{dia} and σ_{so}. A recent theoretical analysis of the Gutmann–Beckett method by Greb *et al.* revealed that the same is true for $\delta(^{31}P)$ in $Et_3PO{\rightarrow}$LA.[127] Nevertheless, the trends in $\delta(^{31}P)$ and $\delta(^{35}Cl)$ go in opposite directions with increasing strength of the Lewis acid: While stronger LAs cause larger *downfield* shifts of the ^{31}P resonances of corresponding $Et_3PO{\rightarrow}$LA adducts, the ^{35}Cl resonances of silafulleranes $[Cl@Si_{20}Y_{20}]^-$ become more *upfield* shifted the more electron-withdrawing the Y substituents are and the stronger the $Cl^-{\rightarrow}Si_{20}$ interaction energy E_{int} becomes (cf. Figure 10). We note in passing that this inverse correlation between $\delta(^{35}Cl)$ and E_{int} is most pronounced for Y = H, F-I, but also holds for the subsets $[Cl@Si_{20}H_{20}]^-{\rightarrow}[Cl@Si_{20}H_{12}Y_8]^-{\rightarrow}[Cl@Si_{20}Y_{20}]^-$ (Y = F-I). In contrast, the less electron-withdrawing substituents Y = Me, Et do not yet lead to a clear trend and require more data points to make robust statements. In addition to the values for the complete silafulleranes $[Cl@Si_{20}Y_{20}]^-$, we have also computed $\delta(^{35}Cl)$ and E_{int} for the non-spherical model systems **Cl-1** to **Cl-9** (Y = Cl; Figure 2) and the analogous subsets with Y = H, F, Br, I. For each subset, we can extrapolate trajectories starting at **Y-1** and approaching the values of the fully assembled $[Cl@Si_{20}Y_{20}]^-$ clusters as the model systems grow bigger (Figure 10). For Y = H, Cl, Br, I, we now see that an increasing E_{int} results in increasingly *deshielded* ^{35}Cl nuclei – analogous to the Gutmann–Beckett scale and inverse to the trend observed for $[Cl@Si_{20}Y_{20}]^-$.[128] Taken together, these results lead to the important conclusion that there does not seem to be a generally valid correlation between $\delta(^{35}Cl)$ and E_{int} for all pairs of Lewis acidic oligosilanes and Cl^- ions. However, for well-defined subsets, such as either $[Cl@Si_{20}Y_{20}]^-$ or **Cl-1** to **Cl-12**, corresponding correlations do exist and are of considerable diagnostic and predictive value.

According to the Ramsey equation, σ_{para} is proportional to the negative inverse of the energy gaps in pairs of magnetically coupled occupied and vacant orbitals.[129,130] For the silafulleranes $[Cl@Si_{20}Y_{20}]^-$ (Y = H, Me, Et, F-I), we conducted a Ditchfield decomposition analysis to reveal the

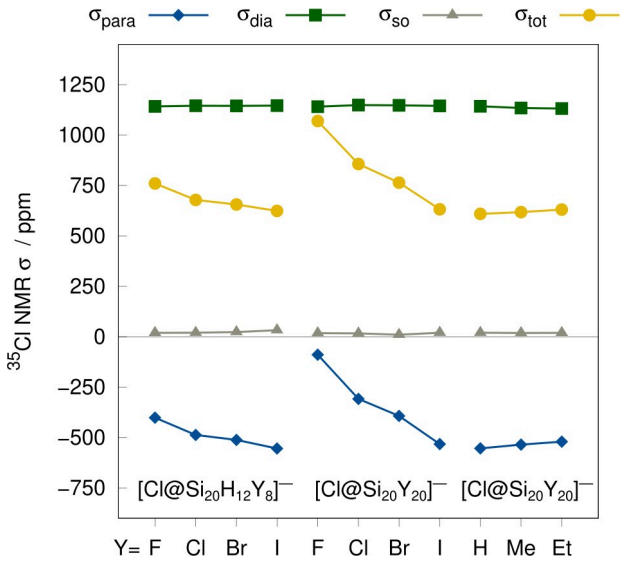

Figure 9. Paramagnetic (σ_{para}), diamagnetic (σ_{dia}), and spin-orbit contributions (σ_{so}) to the total isotropic shielding σ_{tot} of the ^{35}Cl nucleus inside the respective Si_{20} cluster.

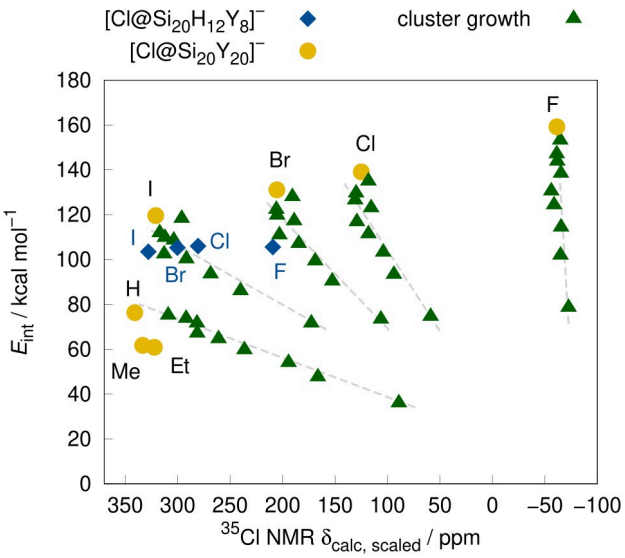

Figure 10. Correlation between the interaction energy (E_{int}) and the calculated and linearly scaled ^{35}Cl NMR chemical shift δ.

contribution of each molecular orbital pair to the paramagnetic shielding.[131–133] In all cases, the main contributions to σ_{para} come from excitations from the electron lone pairs of the endohedral Cl^- ion into vacant orbitals above the LUMO. The corresponding donor-acceptor orbital gaps (ΔE_{DA}) indeed show a good correlation with the paramagnetic ^{35}Cl shielding constants (σ_{para}; Figure 11). Consequently, and in agreement with the experiment, $\delta(^{35}Cl)$ is small when ΔE_{DA} is large because electronegative substituents Y lead to high $Cl^-\rightarrow Si_{20}$ interaction energies E_{int}. If, in a simplified approach, ΔE_{DA} is approximated by the HOMO–LUMO gap ΔE_{HL} of $[Cl@Si_{20}Y_{20}]^-$, the above-mentioned inverse correlation with σ_{para} does no longer apply (Table 2). Thus, a reliable analysis of $\delta(^{35}Cl)$ inevitably requires the laborious consideration of all donor-acceptor orbital pairs because excitation from the HOMO to the LUMO is not the main factor. From our density-deformation computations, we also obtained the contributions of each natural orbital of chemical valence (NOCV) to $\delta(^{35}Cl)$. Along the series of exohedral substituents Y, the respective largest contribution (ΔE_k) correlates with σ_{para} (Y = F-I; Table 2). No obvious interdependence was observed between $\delta(^{35}Cl)$ and the $Cl^-\rightarrow Si_{20}Y_{20}$ charge transfer (CT) or the largest absolute principal component ($|V_{33}|$) of the electric field gradient (EFG), which governs the linewidth of the NMR resonance (Table 2).[134] In conclusion, $\delta(^{35}Cl)$ of our silafulleranes $[Cl@Si_{20}Y_{20}]^-$ correlates inversely with (i) the $Cl^-\rightarrow Si_{20}$ interaction energy E_{int} and in turn the Lewis acidity of the empty $Si_{20}Y_{20}$ cage, and (ii) with the donor-acceptor orbital gaps ΔE_{DA}, but shows no correlation with the $Cl^-\rightarrow Si_{20}Y_{20}$ CT.

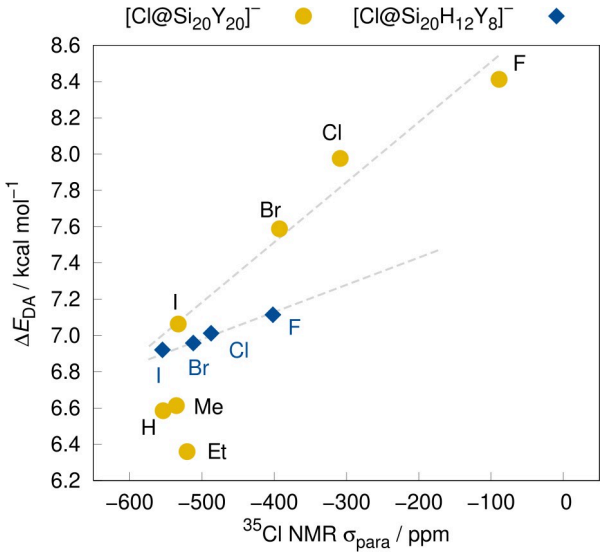

Figure 11. Correlation between the donor-acceptor gap (ΔE_{DA}) and the paramagnetic ^{35}Cl NMR shielding constant σ_{para}.

Introduction of Sterically Demanding Substituents

The primary starting material $[nBu_4N][\mathbf{A}]$ is accessible in a one-pot self-assembly process from Si_2Cl_6, $[nBu_4N]Cl$, and nBu_3N in 27 % yield.[43] Twelvefold desilylation of $[nBu_4N][\mathbf{A}]$ with pinacol, followed by treatment with iBu_2AlH, furnishes $[nBu_4N][Cl@Si_{20}H_{20}]$.[44] Addition of [PPN]Cl to the reaction mixture gives $[PPN][Cl@Si_{20}H_{20}]$ after crystallization ($[PPN]^+ = [(Ph_3P)_2N]^+$). Heating $[PPN][Cl@Si_{20}H_{20}]$ in $CHCl_3$ affords $[PPN][Cl@Si_{20}Cl_{20}]$. For the methylation of $[PPN][Cl@Si_{20}Cl_{20}]$, we adapted the recently described synthesis of $[nBu_4N][Cl@Si_{20}(SiH_3)_{12}Me_8]$,[134] which builds on regioselective Cl/H and Cl/Me exchange in a three-component reaction of $[nBu_4N][\mathbf{A}]$ with Me_2AlH[135] and Me_3Al. The Me_2AlH/Me_3Al system is capable of hydrogenating only the silyl groups of $[\mathbf{A}]^-$, while the Si_{20} core is selectively methylated.[134] In a similar vein, treatment of $[PPN][Cl@Si_{20}Cl_{20}]$ with Me_2AlH/Me_3Al (8/40 equiv.) resulted in the exhaustive methylation of the Si_{20} cluster (Scheme 1a). $[PPN][Cl@Si_{20}Me_{20}]$ was isolated by crystallization from THF in 24 % yield.[136] In the absence of Me_2AlH, a mixture of $[PPN][Cl@Si_{20}Cl_{20}]$ and Me_3Al (40 equiv.) remained unchanged at room temperature for at least 1 d. This result suggests that hydridic H substituents on Al or Si promote core methylation. This conclusion is supported by the fact that $[PPN][Cl@Si_{20}Me_{20}]$ was also formed from a mixture of the chlorosilane $[PPN][Cl@Si_{20}Cl_{20}]$ (1.0 equiv.), the hydridosilane $[PPN][Cl@Si_{20}H_{20}]$ (0.50 equiv.), and Me_3Al (60 equiv.). Following this approach, we also achieved perethylation of a $[PPN][Cl@Si_{20}Cl_{20}]/[PPN][Cl@Si_{20}H_{20}]$ mixture (1.0/0.50 equiv.) with Et_3Al (20 equiv.; Scheme 1a).

Table 2: Different calculated properties for the investigated systems.

	$\delta^{35Cl}_{calc,scaled}$/ppm	σ^{35Cl}_{para}/ppm	EFG $\lvert V_{33}\rvert$/a.u.	ΔE_{HL}/eV	ΔE_{DA}/eV	E_{int}/kcal mol^{-1}	CT/e^{-1}	ΔE_k/kcal mol^{-1}
$[Cl@Si_{20}H_{12}F_8]^-$	209.3	−401.7	0.00106	4.5	7.1	105.6	0.513	−18.4
$[Cl@Si_{20}H_{12}Cl_8]^-$	280.6	−487.1	0.00037	4.6	7.0	106.0	0.492	−18.9
$[Cl@Si_{20}H_{12}Br_8]^-$	300.3	−511.9	0.00115	4.4	7.0	105.3	0.489	−19.1
$[Cl@Si_{20}H_{12}I_8]^-$	328.0	−554.4	0.00069	4.1	6.9	103.5	0.503	−19.7
$[Cl@Si_{20}F_{20}]^-$	−61.4	−88.9	0.00048	3.0	8.4	159.2	0.508	−17.6
$[Cl@Si_{20}Cl_{20}]^-$	124.9	−308.5	0.00035	3.5	8.0	139.1	0.452	−19.1
$[Cl@Si_{20}Br_{20}]^-$	205.4	−392.6	0.00054	3.5	7.6	131.1	0.438	−19.6
$[Cl@Si_{20}I_{20}]^-$	320.9	−532.6	0.00013	3.4	7.1	119.6	0.477	−20.4
$[Cl@Si_{20}H_{20}]^-$	340.9	−553.6	0.00013	5.4	6.6	76.3	0.513	−18.2
$[Cl@Si_{20}Me_{20}]^-$	333.3	−535.2	0.00008	4.7	6.6	61.7	0.504	−19.2
$[Cl@Si_{20}Et_{20}]^-$	322.3	−520.3	0.01025	4.7	6.4	60.9	0.522	−19.0

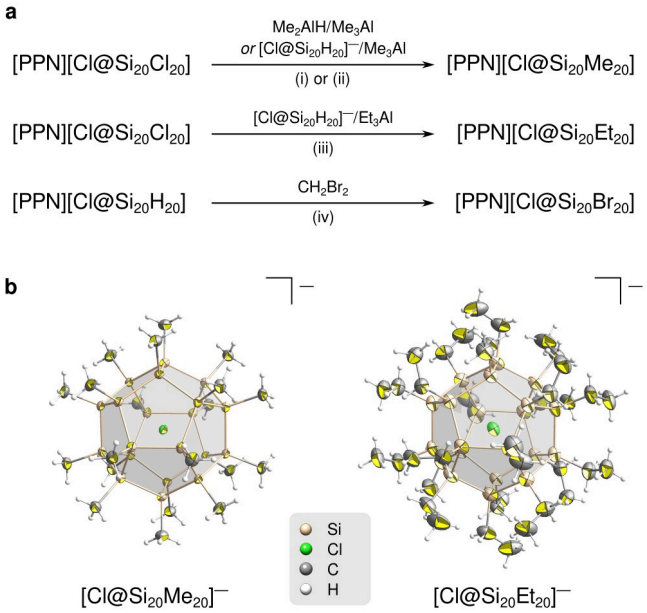

Scheme 1. (a) Syntheses of the siladodecahedrane salts [PPN][Cl@$Si_{20}Y_{20}$] (Y = Me, Et, Br). Reaction conditions: (i) 8 equiv. Me_2AlH, 40 equiv. Me_3Al, *o*DFB/toluene, rt, 15 h. Yield: 24%. (ii) 0.50 equiv. [PPN][Cl@$Si_{20}H_{20}$], 60 equiv. Me_3Al, *o*DFB/toluene, rt, 3 d. Yield: 10%. (iii) 0.50 equiv. [PPN][Cl@$Si_{20}H_{20}$], 20 equiv. Et_3Al, *o*DFB/hexanes, rt, 5 d. Yield: 30%. (iv) CH_2Br_2/C_6D_6 5:1 (380 equiv. CH_2Br_2), 65 °C, 48 h. Yield: 29%. *o*DFB = *ortho*-difluorobenzene. (b) Crystallographically determined structures of the siladodecahedrane salts [PPN][Cl@$Si_{20}Me_{20}$]×THF and [PPN][Cl@$Si_{20}Et_{20}$] in the solid state (the cations and co-crystallized THF are omitted for clarity). Displacement ellipsoids are drawn at the 50% probability level.

[PPN][Cl@$Si_{20}Et_{20}$] was isolated by crystallization from THF in 30% yield.[136]

The conversion of [PPN][Cl@$Si_{20}H_{20}$] to [PPN][Cl@$Si_{20}Cl_{20}$][44] by heating the hydridosilane in $CHCl_3$ served as the role model for the synthesis of [PPN][Cl@$Si_{20}Br_{20}$]: H/Br exchange on [PPN][Cl@$Si_{20}H_{20}$] was achieved by keeping its CH_2Br_2/C_6D_6 (5:1) solution in an NMR tube at 65 °C for 48 h (Scheme 1a). At the endpoint of the reaction, a SiH signal was no longer detectable in the ^{1}H NMR spectrum, and the resonance of the CH_3Br byproduct showed an integral value indicating a 20:1 stoichiometry relative to $[PPN]^+$. After purification by precipitation from *o*DFB with *n*-hexane, [PPN][Cl@$Si_{20}Br_{20}$] was isolated as a yellow solid in 29% yield (Scheme 1a).[137]

In a first investigation of the stability of the siladodecahedrane salts [PPN][Cl@$Si_{20}Y_{20}$] toward Lewis bases, we found that [Cl@$Si_{20}Cl_{20}$]$^-$ and [Cl@$Si_{20}Br_{20}$]$^-$ decompose rapidly in THF ([Cl@$Si_{20}Cl_{20}$]$^-$ is stable in dry MeCN for extended periods of time). In stark contrast, [Cl@$Si_{20}Me_{20}$]$^-$ is not only inert to THF but persists for days even in the presence of the strong F^- donor $[S(NMe_2)_3][Me_3SiF_2]$ (TASF). Apparently, the relatively low computed affinity of the permethylated siladodecahedrane cage for its endohedral Cl^- guest finds its counterpart in a comparably low affinity for attacking exohedral Lewis bases. In contrast, halogenated Si_{20} cages appear to be much more prone to both endohedral and exohedral interactions with Lewis bases. Attempts at the synthesis of [PPN][Cl@$Si_{20}F_{20}$] and [PPN][Cl@$Si_{20}I_{20}$] were of limited success, although we were able to detect the molecular-ion peak of [Cl@$Si_{20}I_{20}$]$^-$ in the mass spectrum (m/z = 3134.66, calcd.: 3134.59; cf. the Supporting Information for more details).

Crystals of [PPN][Cl@$Si_{20}Me_{20}$]×THF suitable for X-ray crystallography grew during the slow evaporation of the above-mentioned [PPN][Cl@$Si_{20}Me_{20}$]/TASF mixture in THF. [PPN][Cl@$Si_{20}Et_{20}$] crystallized from an *ortho*-difluorobenzene/hexanes mixture upon evaporation. The proposed molecular structures of the anions [Cl@$Si_{20}Me_{20}$]$^-$ and [Cl@$Si_{20}Et_{20}$]$^-$ were confirmed (Scheme 1b); however, the structure determination of [PPN][Cl@$Si_{20}Et_{20}$] was challenging due to the pseudo-merohedral twinning of three components[138] and required high-quality data obtained with synchrotron radiation (cf. the Supporting Information for details). The endohedral Cl···Si distances and Si–Si bond lengths in [Cl@$Si_{20}Me_{20}$]$^-$ and [Cl@$Si_{20}Et_{20}$]$^-$ are very similar to the corresponding published values[44] of [Cl@$Si_{20}H_{20}$]$^-$ and [Cl@$Si_{20}Cl_{20}$]$^-$ (Table 3). [Cl@$Si_{20}Me_{20}$]$^-$, [Cl@$Si_{20}Et_{20}$]$^-$, and [Cl@$Si_{20}(SiH_3)_{12}Me_8$]$^-$[134] have essentially identical Si–C bond lengths (Table 3).

The molecular-ion peaks of [Cl@$Si_{20}Y_{20}$]$^-$ (Y = Me, Et, Br, I) with matching isotope patterns were detected by LDI-MS(−). In contrast to [Cl@$Si_{20}Me_{20}$]$^-$ and [Cl@$Si_{20}Et_{20}$]$^-$, which do not appear to undergo significant fragmentation under the applied measurement conditions, [Cl@$Si_{20}Br_{20}$]$^-$ and [Cl@$Si_{20}I_{20}$]$^-$ show cluster fragmentation in the mass spectrometer. In both cases, peaks assignable to smaller clusters $[Si_aY_bCl]^-$ (Y = Br, I; $a,b \leq 20$) were found (cf. the Supporting Information for details).

The NMR spectra of [PPN][Cl@$Si_{20}Me_{20}$]/[PPN][Cl@$Si_{20}Et_{20}$] and [PPN][Cl@$Si_{20}Br_{20}$] were recorded in $[D_8]$THF and CH_2Br_2/C_6D_6 (5:1), respectively (Table 3). [Cl@$Si_{20}Me_{20}$]$^-$ gives singlets at 0.12 ppm and −7.6 ppm (Table 3) in the ^{1}H and $^{13}C\{^1H\}$ NMR spectrum, respectively. The protons of [Cl@$Si_{20}Et_{20}$]$^-$ come to resonance at 1.20–1.11 ppm; two ^{13}C signals were found at 12.8 ppm (CH_3) and 8.5 ppm (CH_2). In accordance with an average I_h symmetry on the NMR time scale, the ^{29}Si NMR spectra showed one resonance for each of the anions [Cl@$Si_{20}Me_{20}$]$^-$ (δ = −30.6 ppm, calcd: −29.7 ppm; Table 3), [Cl@$Si_{20}Et_{20}$]$^-$ (δ = −18.4 ppm, calcd: −13.0 ppm), and [Cl@$Si_{20}Br_{20}$]$^-$ (δ = −22.1 ppm, calcd: −22.3 ppm). In the case of [Cl@$Si_{20}Me_{20}$]$^-$, the J(Si,Cl) coupling constant of 3.4 Hz was determined using a ^{29}Si DEPT-3P experiment (calcd: 3.4 Hz; cf. [Cl@$Si_{20}H_{20}$]$^-$: 3.3 Hz, [Cl@$Si_{20}Cl_{20}$]$^-$: 4.7 Hz).[44] The ^{35}Cl nuclei in [Cl@$Si_{20}Me_{20}$]$^-$ (δ = 332.7 ppm, scaled calcd. value: 333.4 ppm) and [Cl@$Si_{20}Et_{20}$]$^-$ (δ = 326.3, scaled calcd. value: 322.3 ppm) possess chemical shift values similar to that in [Cl@$Si_{20}H_{20}$]$^-$ (δ = 344.9 ppm); significantly stronger ^{35}Cl shielding was observed for [Cl@$Si_{20}Br_{20}$]$^-$ (δ = 210.9 ppm, scaled calcd. value: 205.4 ppm).

Table 3: Selected experimentally determined (calculated) crystallographic and NMR-spectroscopic parameters[a] of the silafulleranes presented herein. Calculated NMR shifts have been computed at the SO-ZORA-PBE0[101] (COSMO(CH_2Cl_2))/ZORA/TZP level of theory.

Compound	d(Cl···Si)/Å	d(Si–Si)/Å	d(Si–C)/Å	δ(^{1}H)	δ(^{13}C)	δ(^{29}Si)	δ(^{35}Cl)
[PPN][Cl@$Si_{20}Me_{20}$]	3.2967(11)–3.3161(8)	2.3522(17)–2.3685(16)	1.896(5)–1.920(3)	0.12	−7.6 (−4.8)	−30.6 (−29.7)	332.7 (333.4)[b]
[PPN][Cl@$Si_{20}Et_{20}$]	3.293(2)–3.3290(18)	2.348(2)–2.381(3)	1.903(5)–1.933(6)	1.20–1.11	12.8 (16.3, CH_3) 8.5 (8.3, CH_2)	−18.4 (−13.0)	326.3 (322.3)[b]
[PPN][Cl@$Si_{20}Br_{20}$]	–	–	–	–	–	−22.1 (−22.3)	210.9 (205.4)[b]
[PPN][Cl@$Si_{20}H_{20}$][44]	3.268(3)–3.314(4)[c]	2.338(5)–2.363(5)[c]	–	3.99	–	−54.7	344.9 (340.9)[b]
[PPN][Cl@$Si_{20}Cl_{20}$][44]	3.293(2)–3.324(2)	2.350(2)–2.368(2)	–	–	–	−21.8[d]	126.0[d] (124.9)[b]
[nBu$_4$N][Cl@$Si_{20}(SiH_3)_{12}Me_8$][134]	3.2541(3)–3.3040(3) (Cl···Si^0) 3.3191(3)–3.3433(3) (Cl···SiMe)	2.3200(5)–2.3377(4) (Si^0–SiH_3) 2.3485(4)–2.3611(4) (Si^0–SiMe) 2.3453(4)–2.3544(4) (Si^0–Si^0)	1.8974(12)–1.9189(13)	0.51 (CH_3) 3.29 (SiH_3)	−2.4	19.1 (SiMe) −67.2 (Si^0) −100.6 (SiH_3)	457.1 (456.2)[b]

[a] NMR spectra were recorded in [D$_8$]THF ([PPN][Cl@$Si_{20}Me_{20}$], [PPN][Cl@$Si_{20}Et_{20}$], [PPN][Cl@$Si_{20}H_{20}$], [nBu$_4$N][Cl@$Si_{20}(SiH_3)_{12}Me_8$]), CH_2Br_2/C_6D_6 (5:1; [PPN][Cl@$Si_{20}Br_{20}$]), or CD_2Cl_2 ([PPN][Cl@$Si_{20}Cl_{20}$]). [b] These values were obtained after scaling according to the following linear equation: $\delta(^{35}Cl, \text{scaled}) = 0.8728 \cdot \delta(^{35}Cl, \text{calcd}) - 7.3179$.[139] [c] These ranges cover the values determined for both the [nBu$_4$N]$^+$ and the [PPN]$^+$ salt of [Cl@$Si_{20}H_{20}$]$^-$. [d] These values were determined for the [nBu$_4$N]$^+$ salt.

Conclusion

We conducted comprehensive quantum chemical and experimental studies to evaluate different compelling properties of [X@$Si_{20}Y_{20}$]$^-$ clusters and introduced the syntheses of the Y = Me, Et, Br derivatives. To find a reasonable level of theory for our computations, we evaluated the performance of different density functional approximations. The hybrid density functional r^{2}SCAN0-D4 in combination with a large and diffuse basis set yields the most accurate results for the tested systems. We elucidated the template effect of endohedral Cl$^-$ ions in the cluster assembly of [20]silafulleranes and investigated the underlying X$^-$→Si_{20} interaction as well as NMR properties of differently substituted [X@$Si_{20}Y_{20}$]$^-$ clusters. To further broaden the experimental basis of our theoretical considerations, the syntheses of compounds [PPN][Cl@$Si_{20}Y_{20}$] (Y = Me, Et, Br) are also described. Through our combined experimental and theoretical efforts, we are becoming increasingly able to synthesize novel silafulleranes in a targeted manner; at the same time, we have developed robust analytical tools to characterize their key properties.

Since intermediates of the cluster assembly are unknown, we studied a hypothetical series of silapolyquinane model systems and their propensity to coordinate a Cl$^-$ ion on their concave side. Our computations revealed that the interaction between the coordinated Cl$^-$ ion and the respective silicon frameworks becomes stronger as the clusters grow, which supports our previous postulate of a structure-determining template effect of the Cl$^-$ ion.

The main contributions to the attractive X$^-$→Si_{20} interaction energy (E_{int}) in [X@$Si_{20}Y_{20}$]$^-$ clusters stem from electrostatic and orbital-interaction effects. E_{int} is influenced by a cooperative effect between the endohedral ion X$^-$ and the exohedral substituent Y. It is maximized if X$^-$ has the proper size and Y is strongly electron-withdrawing. We investigated different steric effects and found that endohedral ions bigger than Cl$^-$ lead to a larger cage strain and eventually to an expansion of the cage. As it is not feasible to extract the endohedral ion from the cage, we consider [X@$Si_{20}Y_{20}$]$^-$ clusters as confined Lewis pairs.

Further, we verified that the ^{35}Cl NMR shift of an endohedral Cl$^-$ ion is a probe for E_{int} in halogenated Si_{20} cages and we could draw similarities and differences to the prominent Gutmann–Beckett method. The main contribution to the ^{35}Cl NMR chemical shift is the paramagnetic shielding constant σ_{para}. Therefore, $\delta(^{35}Cl)$ is smaller for large donor-acceptor orbital gaps, which occur when the cage bears electronegative substituents.

With the newly found properties, the differently substituted [20]silafulleranes could, e.g., be used as weakly coordinating anions (WCA) or as building blocks for reticular assemblies in future applications.

Acknowledgements

M.Ba. wishes to thank the Fonds der Chemischen Industrie (FCI) for a Kekulé Ph.D. grant. S.G. and M.Bu. gratefully acknowledge financial support from the Max Planck Society through the Max Planck Fellow program. M.W. thanks the Deutsche Forschungsgemeinschaft for financial support (DFG grant no. 506550642). The authors are grateful to Evonik Operations GmbH, Rheinfelden (Germany), for the

generous donation of Si_2Cl_6. Parts of this research (project I-20220822) were carried out at PETRA III at DESY, a member of the Helmholtz Association (HGF). A.V. and M.Ba. thank Dr. Leila Noohinejad, Dr. Martin Tolkiehn, and Dr. Eugenia Peresypkina for their assistance regarding the use of the beamline P24. A.V. thanks Dr. Matthias Meyer (Rigaku Oxford Diffraction) for his precious help with the implementation of the CrysAlisPro software for the synchrotron and STOE IPDS II diffraction data. T.G. thanks Christoph Plett for fruitful discussions. M.Ba. thanks Prof. Dr. Lutz Greb for helpful discussions. Open Access funding enabled and organized by Projekt DEAL.

Conflict of Interest

The authors declare no competing financial interest.

Data Availability Statement

The data that support the findings of this study are available in the supplementary material of this article.

Keywords: ^{35}Cl NMR · Confined Lewis Pairs · Coupled-Cluster · DFT · Silafulleranes

[1] C. Marschner, T. D. Tilley, *Dalton Trans.* **2017**, *46*, 8699.
[2] N. Wiberg, C. M. M. Finger, K. Polborn, *Angew. Chem. Int. Ed.* **1993**, *32*, 1054.
[3] H. Matsumoto, K. Higuchi, Y. Hoshino, H. Koike, Y. Naoi, Y. Nagai, *J. Chem. Soc. Chem. Commun.* **1988**, *3*, 1083.
[4] J. Fischer, J. Baumgartner, C. Marschner, *Science* **2005**, *310*, 825.
[5] H. W. Kroto, J. R. Heath, S. C. O'Brien, R. F. Curl, R. E. Smalley, *Nature* **1985**, *318*, 162.
[6] R. F. Curl, R. E. Smalley, *Science* **1988**, *242*, 1017.
[7] W. Krätschmer, L. D. Lamb, K. Fostiropoulos, D. R. Huffman, *Nature* **1990**, *347*, 354.
[8] H. Prinzbach, A. Weiler, P. Landenberger, F. Wahl, J. Wörth, L. T. Scott, M. Gelmont, D. Olevano, B. v. Issendorff, *Nature* **2000**, *407*, 60.
[9] W. Krätschmer, *Nanoscale* **2011**, *3*, 2485.
[10] R. J. Ternansky, D. W. Balogh, L. A. Paquette, *J. Am. Chem. Soc.* **1982**, *104*, 4503.
[11] J. C. Grossman, L. Mitáš, *Phys. Rev. Lett.* **1995**, *74*, 1323.
[12] K.-M. Ho, A. A. Shvartsburg, B. Pan, Z.-Y. Lu, C.-Z. Wang, J. G. Wacker, J. L. Fye, M. F. Jarrold, *Nature* **1998**, *392*, 582.
[13] B.-x. Li, P.-l. Cao, *Phys. Rev. A* **2000**, *62*, 023201.
[14] I. Rata, A. A. Shvartsburg, M. Horoi, T. Frauenheim, K. W. M. Siu, K. A. Jackson, *Phys. Rev. Lett.* **2000**, *85*, 546.
[15] B.-x. Li, P.-l. Cao, *J. Phys. Condens. Matter* **2001**, *13*, 10865.
[16] Unsaturated silicon clusters containing non-substituted cluster vertices are mainly known in the form of Zintl ions and siliconoids: a) Y. Heider, D. Scheschkewitz, *Chem. Rev.* **2021**, *121*, 9674; b) D. Scheschkewitz, *Angew. Chem. Int. Ed.* **2005**, *44*, 2954; c) J. Keuter, C. Schwermann, A. Hepp, K. Bergander, J. Droste, M. R. Hansen, N. L. Doltsinis, C. Mück-Lichtenfeld, F. Lips, *Chem. Sci.* **2020**, *11*, 5895; d) S. Scharfe, F. Kraus, S. Stegmaier, A. Schier, T. F. Fässler, *Angew. Chem. Int. Ed.* **2011**, *50*, 3630; e) S. Joseph, M. Hamberger, F. Mutzbauer, O. Härtl, M. Meier, N. Korber, *Angew. Chem. Int. Ed.* **2009**, *48*, 8770.
[17] K. Jackson, B. Nellermoe, *Chem. Phys. Lett.* **1996**, *254*, 249.
[18] Q. Sun, Q. Wang, T. M. Briere, V. Kumar, Y. Kawazoe, P. Jena, *Phys. Rev. B: Condens. Matter Mater. Phys.* **2002**, *65*, 235417.
[19] T. Nagano, K. Tsumuraya, H. Eguchi, D. J. Singh, *Phys. Rev. B: Condens. Matter Mater. Phys.* **2001**, *64*, 155403.
[20] A. K. Singh, V. Kumar, Y. Kawazoe, *Phys. Rev. B: Condens. Matter Mater. Phys.* **2005**, *71*, 115429.
[21] J.-P. Dognon, C. Clavaguéra, P. Pyykkö, *Chem. Sci.* **2012**, *3*, 2843.
[22] This formal charge assignment does not claim to reflect the actual charge distribution in the molecule.
[23] S. Nagase, *Acc. Chem. Res.* **1995**, *28*, 469.
[24] L. Silaghi-Dumitrescu, A. Kun, I. Haiduc, *Fullerene Sci. Technol.* **1999**, *7*, 841.
[25] F. Pichierri, V. Kumar, *J. Mol. Struct.: THEOCHEM* **2009**, *900*, 71.
[26] A. D. Zdetsis, *Phys. Rev. B: Condens. Matter Mater. Phys.* **2009**, *80*, 195417.
[27] M. Anafcheh, R. Ghafouri, N. L. Hadipour, *Phys. E* **2012**, *44*, 2099.
[28] E. N. Koukaras, A. D. Zdetsis, P. Karamanis, C. Pouchan, A. Avramopoulos, M. G. Papadopoulos, *J. Comput. Chem.* **2012**, *33*, 1068.
[29] F. Marsusi, M. Qasemnazhand, *Nanotechnology* **2016**, *27*, 275704.
[30] C. W. Earley, *J. Phys. Chem. A* **2000**, *104*, 6622.
[31] V. Kumar, Y. Kawazoe, *Phys. Rev. Lett.* **2003**, *90*, 055502.
[32] F. Pichierri, V. Kumar, Y. Kawazoe, *Chem. Phys. Lett.* **2004**, *383*, 544.
[33] G. Ramachandran, S. Manogaran, *J. Mol. Struct.: THEOCHEM* **2005**, *730*, 171.
[34] A. J. Karttunen, M. Linnolahti, T. A. Pakkanen, *J. Phys. Chem. C* **2007**, *111*, 2545.
[35] Y. Pei, Y. Gao, X. C. Zeng, *J. Chem. Phys.* **2007**, *127*, 044704.
[36] B.-C. Wang, Y.-M. Chou, J.-P. Deng, Y.-T. Dung, *J. Phys. Chem. A* **2008**, *112*, 6351.
[37] H. Wang, L. Wu, *Chin. J. Chem.* **2011**, *29*, 2063.
[38] D. Palagin, K. Reuter, *ACS Nano* **2013**, *7*, 1763.
[39] F. Pichierri, V. Kumar, Y. Kawazoe, *Chem. Phys. Lett.* **2005**, *406*, 341.
[40] D. Palagin, K. Reuter, *Phys. Rev. B: Condens. Matter Mater. Phys.* **2012**, *86*, 045416.
[41] C.-Y. Zhang, H.-S. Wu, *J. Mol. Struct.: THEOCHEM* **2006**, *770*, 145.
[42] C.-Y. Zhang, H.-S. Wu, H. Jiao, *Chem. Phys. Lett.* **2005**, *410*, 457.
[43] J. Tillmann, J. H. Wender, U. Bahr, M. Bolte, H.-W. Lerner, M. C. Holthausen, M. Wagner, *Angew. Chem. Int. Ed.* **2015**, *54*, 5429.
[44] M. Bamberg, M. Bursch, A. Hansen, M. Brandl, G. Sentis, L. Kunze, M. Bolte, H.-W. Lerner, S. Grimme, M. Wagner, *J. Am. Chem. Soc.* **2021**, *143*, 10865.
[45] D. S. De, B. Schaefer, B. v. Issendorff, S. Goedecker, *Phys. Rev. B: Condens. Matter Mater. Phys.* **2020**, *101*, 214303.
[46] M. Ponce-Vargas, A. Muñoz-Castro, *J. Phys. Chem. C* **2018**, *122*, 12551.
[47] F. Neese, F. Wennmohs, U. Becker, C. Riplinger, *J. Chem. Phys.* **2020**, *152*, 224108.
[48] C. Bannwarth, E. Caldeweyher, S. Ehlert, A. Hansen, P. Pracht, J. Seibert, S. Spicher, S. Grimme, *Wiley Interdiscip. Rev.: Comput. Mol. Sci.* **2021**, *11*, e1493.
[49] TURBOMOLE V7.3 2018, a development of University of Karlsruhe and Forschungszentrum Karlsruhe GmbH, 1989–

2007, TURBOMOLE GmbH, since 2007; available from http://www.turbomole.com.
[50] H.-J. Werner, P. J. Knowles, F. R. Manby, J. A. Black, K. Doll, A. Heßelmann, D. Kats, A. Köhn, T. Korona, D. A. Kreplin, Q. Ma, T. F. Miller, A. Mitrushchenkov, K. A. Peterson, I. Polyak, G. Rauhut, M. Sibaev, *J. Chem. Phys.* **2020**, *152*, 144107.
[51] H.-J. Werner, P. J. Knowles, P. Celani, W. Györffy, A. Hesselmann, D. Kats, G. Knizia, A. Köhn, T. Korona, D. Kreplin, R. Lindh, Q. Ma, F. R. Manby, A. Mitrushenkov, G. Rauhut, M. Schütz, K. R. Shamasundar, T. B. Adler, R. D. Amos, S. J. Bennie, A. Bernhardsson, A. Berning, J. A. Black, P. J. Bygrave, R. Cimiraglia, D. L. Cooper, D. Coughtrie, M. J. O. Deegan, A. J. Dobbyn, K. Doll, M. Dornbach, F. Eckert, S. Erfort, E. Goll, C. Hampel, G. Hetzer, J. G. Hill, M. Hodges, T. Hrenar, G. Jansen, C. Köppl, C. Kollmar, S. J. R. Lee, Y. Liu, A. W. Lloyd, R. A. Mata, A. J. May, B. Mussard, S. J. Mc-Nicholas, W. Meyer, T. F. Miller III, M. E. Mura, A. Nicklass, D. P. O'Neill, P. Palmieri, D. Peng, K. A. Peterson, K. Pflüger, R. Pitzer, I. Polyak, M. Reiher, J. O. Richardson, J. B. Robinson, B. Schröder, M. Schwilk, T. Shiozaki, M. Sibaev, H. Stoll, A. J. Stone, R. Tarroni, T. Thorsteinsson, J. Toulouse, M. Wang, M. Welborn, B. Ziegler, MOLPRO, 2022.3, a package of ab initio programs.
[52] G. te Velde, F. M. Bickelhaupt, E. J. Baerends, C. Fonseca Guerra, S. J. A. van Gisbergen, J. G. Snijders, T. Ziegler, *J. Comput. Chem.* **2001**, *22*, 931.
[53] U. Mayer, V. Gutmann, W. Gerger, *Monatsh. Chem.* **1975**, *106*, 1235.
[54] M. A. Beckett, G. C. Strickland, J. R. Holland, K. S. Varma, *Polymer* **1996**, *37*, 4629.
[55] J. Tillmann, L. Meyer, J. I. Schweizer, M. Bolte, H.-W. Lerner, M. Wagner, M. C. Holthausen, *Chem. Eur. J.* **2014**, *20*, 9234.
[56] S.-B. Choi, B.-K. Kim, P. Boudjouk, D. G. Grier, *J. Am. Chem. Soc.* **2001**, *123*, 8117.
[57] X. Dai, D. L. Schulz, C. W. Braun, A. Ugrinov, P. Boudjouk, *Organometallics* **2010**, *29*, 2203.
[58] X. Dai, K. J. Anderson, D. L. Schulz, P. Boudjouk, *Dalton Trans.* **2010**, *39*, 11188.
[59] X. Dai, S.-B. Choi, C. W. Braun, P. Vaidya, S. Kilina, A. Ugrinov, D. L. Schulz, P. Boudjouk, *Inorg. Chem.* **2011**, *50*, 4047.
[60] K. Pokhodnya, C. Olson, X. Dai, D. L. Schulz, P. Boudjouk, A. P. Sergeeva, A. I. Boldyrev, *J. Chem. Phys.* **2011**, *134*, 014105.
[61] J. Tillmann, F. Meyer-Wegner, A. Nadj, J. Becker-Baldus, T. Sinke, M. Bolte, M. C. Holthausen, M. Wagner, H.-W. Lerner, *Inorg. Chem.* **2012**, *51*, 8599.
[62] A. Robertazzi, J. A. Platts, P. Gamez, *ChemPhysChem* **2014**, *15*, 912.
[63] K. Pokhodnya, K. Anderson, S. Kilina, N. Dandu, P. Boudjouk, *J. Phys. Chem. A* **2018**, *122*, 4067.
[64] J. Teichmann, B. Köstler, J. Tillmann, M. Moxter, R. Kupec, M. Bolte, H.-W. Lerner, M. Wagner, *Z. Anorg. Allg. Chem.* **2018**, *644*, 956.
[65] J. Yang, B. Chatelet, V. Dufaud, D. Hérault, S. Michaud-Chevallier, V. Robert, J.-P. Dutasta, A. Martinez, *Angew. Chem. Int. Ed.* **2018**, *57*, 14212.
[66] C. Li, A.-D. Manick, J.-P. Dutasta, X. Bugaut, B. Chatelet, A. Martinez, *Org. Chem. Front.* **2022**, *9*, 1826.
[67] S. Grimme, J. G. Brandenburg, C. Bannwarth, A. Hansen, *J. Chem. Phys.* **2015**, *143*, 054107.
[68] A. V. Marenich, C. J. Cramer, D. G. Truhlar, *J. Phys. Chem. B* **2009**, *113*, 6378.
[69] For an overview of organic polyquinane chemistry, see: L. A. Paquette, The development of polyquinane chemistry, in *Organic Chemistry*, Springer Berlin Heidelberg, Berlin, Heidelberg **1979**, pages 41–165.
[70] A. Tsurusaki, Y. Koyama, S. Kyushin, *J. Am. Chem. Soc.* **2017**, *139*, 3982.
[71] W. B. Schneider, G. Bistoni, M. Sparta, M. Saitow, C. Riplinger, A. A. Auer, F. Neese, *J. Chem. Theory Comput.* **2016**, *12*, 4778.
[72] G. Bistoni, *WIREs Comput. Mol. Sci.* **2020**, *10*, e1442.
[73] A. Altun, M. Saitow, F. Neese, G. Bistoni, *J. Chem. Theory Comput.* **2019**, *15*, 1616.
[74] C. Riplinger, F. Neese, *J. Chem. Phys.* **2013**, *138*, 034106.
[75] C. Riplinger, B. Sandhoefer, A. Hansen, F. Neese, *J. Chem. Phys.* **2013**, *139*, 134101.
[76] C. Riplinger, P. Pinski, U. Becker, E. F. Valeev, F. Neese, *J. Chem. Phys.* **2016**, *144*, 024109.
[77] M. Saitow, U. Becker, C. Riplinger, E. F. Valeev, F. Neese, *J. Chem. Phys.* **2017**, *146*, 164105.
[78] Y. Guo, C. Riplinger, U. Becker, D. G. Liakos, Y. Minenkov, L. Cavallo, F. Neese, *J. Chem. Phys.* **2018**, *148*, 011101.
[79] Q. Ma, H.-J. Werner, *J. Chem. Theory Comput.* **2021**, *17*, 902.
[80] Q. Ma, H.-J. Werner, *WIREs Comput. Mol. Sci.* **2018**, *8*, e1371.
[81] Q. Ma, M. Schwilk, C. Köppl, H.-J. Werner, *J. Chem. Theory Comput.* **2017**, *13*, 4871.
[82] To generate reliable reference interaction energies (E_{int}), we applied a high-level, state-of-the-art local coupled cluster method including explicit correlation (PNO-LCCSD(T)-F12b employed with tight domain settings) with a modified aug-cc-pVQZ basis set (aug-cc-pVQZ-PP for the heavier elements, cc-pVQZ for H; denoted AVQZ' in the following). Since this setup is computationally too expensive for the larger structures (and those with many heavier elements), we applied a slightly less accurate but clearly faster reference protocol (PNO-LCCSD(T)-F12b/AVTZ' with default domain settings) for the latter systems. The respective additional error could be significantly reduced by applying a scaling factor to the triples contributions (see Computational Details in Supporting Information). The, in this way, obtained interaction energies for the subset comprised of the smaller systems are virtually identical to the respective PNO-LCCSD(T)-F12b/AVQZ'/tight results with a mean unsigned error of only 0.05 kcal mol^{-1} (see Supporting Information, Table S1), so that comparably accurate reference values could also be generated for the larger subset. We conservatively estimate the residual error of the generated reference values to be 0.5–1.0 kcal mol^{-1} for E_{int}, thus allowing for a statistical discriminability of about 0.1 kcal mol^{-1} of the mean errors for the evaluated DFT methods.
[83] H.-J. Werner, A. Hansen, *J. Chem. Theory Comput.* **2023**, *19*, 7007.
[84] N. B. Balabanov, K. A. Peterson, *J. Chem. Phys.* **2005**, *123*, 064107.
[85] K. A. Peterson, D. Figgen, M. Dolg, H. Stoll, *J. Chem. Phys.* **2007**, *126*, 124101.
[86] T. H. Dunning, *J. Chem. Phys.* **1989**, *90*, 1007.
[87] A. Klamt, G. Schüürmann, *J. Chem. Soc. Perkin Trans. 2* **1993**, 799.
[88] M. Cossi, N. Rega, G. Scalmani, V. Barone, *J. Comput. Chem.* **2003**, *24*, 669.
[89] A. Klamt, *J. Phys. Chem.* **1995**, *99*, 2224.
[90] COSMO-RS: From Quantum Chemistry to Fluid Phase Thermodynamics and Drug Design, in Klamt (Editor), *COSMO-RS: From Quantum Chemistry to Fluid Phase Thermodynamics and Drug Design*, pages 1–234, Elsevier, Amsterdam **2005**.
[91] S. Grimme, *Chem. Eur. J.* **2012**, *18*, 9955.

[92] We tested the following density functional approximations in combination the the ma-def2-QZVPP basis set: PBE-D4, TPSS-D4, PW6B95-D4, B3LYP-D4, PBE0-D4, r^{2}SCAN0-D4, ωB97X-D4, ωB97X-V, ωB97M-D4, ωB97M-V, ωB97X-2-D4, B2PLYP-D4 and PWPB95-D4. Further, the composite r^{2}SCAN-3c DFT method was tested with the def2-mTZVPP basis set.
[93] J. P. Perdew, K. Burke, M. Ernzerhof, *Phys. Rev. Lett.* **1996**, *77*, 3865.
[94] E. Caldeweyher, C. Bannwarth, S. Grimme, *J. Chem. Phys.* **2017**, *147*, 034112.
[95] E. Caldeweyher, S. Ehlert, A. Hansen, H. Neugebauer, S. Spicher, C. Bannwarth, S. Grimme, *J. Chem. Phys.* **2019**, *150*, 154122.
[96] J. Tao, J. P. Perdew, V. N. Staroverov, G. E. Scuseria, *Phys. Rev. Lett.* **2003**, *91*, 146401.
[97] Y. Zhao, D. G. Truhlar, *J. Phys. Chem. A* **2005**, *109*, 5656.
[98] C. Lee, W. Yang, R. G. Parr, *Phys. Rev. B: Condens. Matter Mater. Phys.* **1988**, *37*, 785.
[99] A. D. Becke, *J. Chem. Phys.* **1993**, *98*, 5648.
[100] P. J. Stephens, F. J. Devlin, C. F. Chabalowski, M. J. Frisch, *J. Phys. Chem.* **1994**, *98*, 11623.
[101] C. Adamo, V. Barone, *J. Chem. Phys.* **1999**, *110*, 6158.
[102] M. Bursch, H. Neugebauer, S. Ehlert, S. Grimme, *J. Chem. Phys.* **2022**, *156*, 134105.
[103] A. Najibi, L. Goerigk, *J. Comput. Chem.* **2020**, *41*, 2562.
[104] N. Mardirossian, M. Head-Gordon, *Phys. Chem. Chem. Phys.* **2014**, *16*, 9904.
[105] N. Mardirossian, M. Head-Gordon, *J. Chem. Phys.* **2016**, *144*, 214110.
[106] J.-D. Chai, M. Head-Gordon, *J. Chem. Phys.* **2009**, *131*, 174105.
[107] S. Grimme, *J. Chem. Phys.* **2006**, *124*, 034108.
[108] L. Goerigk, S. Grimme, *J. Chem. Theory Comput.* **2011**, *7*, 291.
[109] J. Zheng, X. Xu, D. G. Truhlar, *Theor. Chem. Acc.* **2011**, *128*, 295.
[110] S. Grimme, A. Hansen, S. Ehlert, J. M. Mewes, *J. Chem. Phys.* **2021**, *154*, 064103.
[111] D. Rappoport, F. Furche, *J. Chem. Phys.* **2010**, *133*, 134105.
[112] F. Weigend, R. Ahlrichs, *Phys. Chem. Chem. Phys.* **2005**, *7*, 3297.
[113] P. Su, H. Li, *J. Chem. Phys.* **2009**, *131*, 014102.
[114] M. Mitoraj, A. Michalak, *J. Mol. Model.* **2007**, *13*, 347.
[115] A. Michalak, M. Mitoraj, T. Ziegler, *J. Phys. Chem. A* **2008**, *112*, 1933.
[116] T. Ziegler, A. Rauk, *Theor. Chim. Acta* **1977**, *46*, 1.
[117] M. P. Mitoraj, A. Michalak, T. Ziegler, *J. Chem. Theory Comput.* **2009**, *5*, 962.
[118] D. MacLeod-Carey, P. L. Rodríguez-Kessler, A. Muñoz-Castro, *Phys. Chem. Chem. Phys.* **2023**, *25*, 19845.
[119] S. K. Wolff, T. Ziegler, *J. Chem. Phys.* **1998**, *109*, 895.
[120] G. Schreckenbach, T. Ziegler, *J. Phys. Chem.* **1995**, *99*, 606.
[121] H. Fukui, *Prog. Nucl. Magn. Reson. Spectrosc.* **1997**, *31*, 317.
[122] C. Chang, M. Pelissier, P. Durand, *Phys. Scr.* **1986**, *34*, 394.
[123] E. van Lenthe, E. J. Baerends, J. G. Snijders, *J. Chem. Phys.* **1993**, *99*, 4597.
[124] E. van Lenthe, E. J. Baerends, J. G. Snijders, *J. Chem. Phys.* **1994**, *101*, 9783.
[125] E. van Lenthe, E. J. Baerends, *J. Comput. Chem.* **2003**, *24*, 1142.
[126] C. C. Pye, T. Ziegler, E. van Lenthe, J. N. Louwen, *Can. J. Chem.* **2009**, *87*, 790.
[127] P. Erdmann, L. Greb, *Angew. Chem. Int. Ed.* **2022**, *61*, e202114550.
[128] For Y = F, we find no such correlation between E_{int} and $\delta(^{35}Cl)$. However, in this case $\triangle\delta(^{35}Cl)$ is rather small between the different cluster sizes, and the same is true for the absolute $\delta(^{35}Cl)$ values, so that any systematic trends can easily be obscured by inaccuracies inherent to the theoretical method.
[129] J. C. Facelli, *Concepts Magn. Reson.* **2004**, *20A*, 42.
[130] J. Gauss, U. Schneider, R. Ahlrichs, C. Dohmeier, H. Schnöckel, *J. Am. Chem. Soc.* **1993**, *115*, 2402.
[131] J. Autschbach, *J. Chem. Phys.* **2008**, *128*, 164112.
[132] R. Ditchfield, *Mol. Phys.* **1974**, *27*, 789.
[133] K. Wolinski, J. F. Hinton, P. Pulay, *J. Am. Chem. Soc.* **1990**, *112*, 8251.
[134] M. Bamberg, T. Gasevic, M. Bolte, A. Virovets, H.-W. Lerner, S. Grimme, M. Bursch, M. Wagner, *J. Am. Chem. Soc.* **2023**, *145*, 11440.
[135] As reported previously,[134] our synthesis leads to a product with the composition $Me_{2.2}AlH_{0.8}$. For simplicity, we refer to the idealized formula Me_2AlH in the main text, but we use the exact stoichiometry in the Supporting Information.
[136] CIF files containing the crystallographic information were deposited in the Cambridge Crystallographic Data Centre under the deposition codes CCDC 2294476 ([PPN][Cl@$Si_{20}Me_{20}$]×THF), CCDC 2294477 ([PPN][Cl@$Si_{20}Et_{20}$]), and CCDC 2294478 ([nBu$_4$N]$_2$[$Si_6I_{10.85}Cl_{1.15}$·2I]; cf. the Supporting Information for details) and can be obtained free of charge via www.ccdc.cam.ac.uk/data_request/cif.
[137] The actual conversion to [PPN][Cl@$Si_{20}Br_{20}$] is about 90 %; the purification step served to remove traces of unknown impurities.
[138] R. Herbst-Irmer, G. M. Sheldrick, *Acta Crystallogr. Sect. B* **1998**, *54*, 443.
[139] M. Bamberg, T. Gasevic, M. Bolte, A. Virovets, H.-W. Lerner, S. Grimme, M. Bursch, M. Wagner, *Chem. Commun.* **2023**, *59*, 7459.

Manuscript received: September 27, 2023
Accepted manuscript online: December 7, 2023
Version of record online: January 2, 2024